Multifragmentation and the Phase Transition: A Systematic Study of the MF of 1A GeV Au, La, and Kr

B. K. Srivastava[1], R. P. Scharenberg[1], S. Albergo[2], F. Bieser[6], F. P. Brady[3], Z. Caccia[2], D. A. Cebra[3], A. D. Chacon[7], J. L. Chance[3], Y. Choi[1], S. Costa[2], J. B. Elliott[1], M. L. Gilkes[1], J. A. Hauger[1], A. S. Hirsch[1], E. L. Hjort[1], A. Insolia[2], M. Justice[5], D. Keane[5], J. C. Kintner[3], V. Lindenstruth[4], M. A. Lisa[6], H. S. Matis[6], M. McMahan[6], C. McParland[6], W. F. J. Müller[4], D. L. Olson[6], M. D. Partlan[3], N. T. Porile[1], R. Potenza[2], G. Rai[6], J. Rasmussen[6], H. G. Ritter[6], J. Romanski[2], J. L. Romero[3], G. V. Russo[2], H. Sann[4], A. Scott[5], Y. Shao[5], T. J. M. Symons[6], M. Tincknell[1], C. Tuvé[2], S. Wang[5], P. Warren[1], H. H. Wieman[6], T. Wienold[6], and K. Wolf[7]

(EOS Collaboration)

[1] *Purdue University, West Lafayette, IN 47907*

[2] *Universitá di Catania and Istituto Nazionale di Fisica Nucleare-Sezione di Catania, 95129 Catania, Italy*

[3] *University of California, Davis, CA 95616*

[4] *GSI, D-64220 Darmstadt, Germany*

[5] *Kent State University, Kent, OH 44242*

[6] *Nuclear Science Division, Lawrence Berkeley National Laboratory, Berkeley, CA 94720*

[7] *Texas A&M University, College Station, TX 77843*

(August 17, 2018)

Abstract

A systematic analysis of the multifragmentation (MF) in fully reconstructed events from 1A GeV Au, La and Kr collisions with C has been performed. This data is used to provide a definitive test of the variable volume version of the statistical multifragmentation model (SMM). A single set of SMM param-

eters directly determined by the data and the semi-empirical mass formula are used after the adjustable inverse level density parameter, ϵ_o is determined by the fragment distributions. The results from SMM for second stage multiplicity, size of the biggest fragment and the intermediate mass fragments are in excellent agreement with the data. Multifragmentation thresholds have been obtained for all three systems using SMM prior to secondary decay. The data indicate that both thermal excitation energy E^*_{th} and the isotope ratio temperature T_{He-DT} decrease with increase in system size at the critical point. The breakup temperature obtained from SMM also shows the same trend as seen in the data. The SMM model is used to study the nature of the MF phase transition. The caloric curve for Kr exhibits back-bending (finite latent heat) while the caloric curves for Au and La are consistent with a continuous phase transition (nearly zero latent heat) and the values of the critical exponents τ, β and γ, both from data and SMM, are close to those for a 'liquid-gas' system for Au and La. We conclude that the larger Coulomb expansion energy in Au and La reduces the latent heat required for MF and changes the nature of the phase transition. Thus the Coulomb energy plays a major role in nuclear MF.

I. INTRODUCTION

During the past decade a large effort has been made to understand the multifragmentation (MF) process in heavy ion reactions. Recently a number of review articles have appeared describing the details of this phenomenon [1–7]. The Purdue group was the first to suggest that nuclear MF might be a critical phenomenon - a second order phase transition occurring near a critical point [8,9]. In an inclusive experiment performed at Fermilab, the spectra of mass identified fragments resulting from proton interactions with both Kr and Xe gas targets were measured [8,9]. The discovery that the yields of fragments with mass A_f produced in p+Kr and p+Xe reactions, with proton beam energy from 80 to 350 GeV, obeyed a power law $Y(A_f) \sim A_f^{-\tau}$, with $\tau \sim 2.5$ [9] generated theoretical interest in MF in terms of a continuous phase transition. A similar power law was also predicted by Fisher [10] for a mass distribution of droplets at a liquid-gas phase transition critical point. Thus the results from the Purdue work gave a hint that MF could provide important information about the equation of state of nuclear matter [11–14]. The analysis of the fragment kinetic energy spectra suggested that the fragments are emitted from a less than normal density system in the decay of a common remnant which is lighter than the target [9,15–17]. An analysis of the fragment yields based on a thermal liquid drop model gave a freeze-out temperature of ~ 5 MeV [9,17]. Similar results were observed when the above study was extended to lower energies [18,19]. This view was supported by exclusive emulsion MF data [20], which were analyzed by Campi to show that the conditional moments of the individual fragment events exhibited characteristics of a phase transition [21–23]. Bauer and Campi were the first to apply the methods used in percolation studies to analyze MF data [21–25]. In percolation theory the moments of the cluster distribution contain the signature of critical behavior [26,27].

In recent years further progress was made by experiments in which practically all the fragments emitted in a given event were detected, thereby permitting complete reconstruction of MF events [28–35]. The ALADIN Collaboration studied the MF of 400A-1000A MeV

Xe, Au, and U nuclei on various targets. Their results showed that fragment yields were independent of the entrance channel when the data were scaled for projectile or target mass [28–30]. The EOS Collaboration studied the MF of 1A GeV gold on carbon and analyzed the data using methods developed in the study of critical phenomena [36–42]. Several critical exponents were determined and their values suggested that the MF of Au can be understood as due to a continuous phase transition [43,44]. The first results of the MF of 1A GeV La and Kr on carbon have also been reported [45,46]. The MF transition appears to involve the breakup of a nucleus to form several IMF's. The production of nucleons and light particles - the nuclear analog of a gas- occurs largely in the fragment deexcitation step [47]. Along with the earlier inclusive studies, these experiments suggested that prior to MF the remnant formed in the prompt stage achieves thermal equilibrium. A two step process was proposed for the collision. This two step process is an idealization of a time dependent process. In the first prompt stage nucleons are knocked out of the participants. The emission of these prompt particle leaves an equilibrated remnant nucleus which undergoes deexcitation in a second step.

In the EOS experiment prompt stage was separated from the MF stage by making a cut on the kinetic energy of light charged particles [39]. This separation was made possible by the ability of the EOS detector to measure nearly all the charged particles and fragments emitted in each event using reverse kinematics [39]. Complete reconstruction and stage separation was therefore possible for a majority of the events. These reconstructed events were characterized by mass, charge, and excitation energy of the remnant. The resultant remnant then undergoes MF to produce excited fragments which then undergo secondary decay to produce the observed fragments [47]. The ALADIN experiment is also capable of measuring all the charged particles except for Z=1 particles [28–30]. The ISiS Collaboration has also produced one of the most complete MF data sets in the high energy collision of p, $\bar{p}$, and π^- with gold [32–35]. In the ISiS experiment the charge and mass of the excited source were obtained on an event by event basis by subtracting the non equilibrium particles from the target charge and mass. However, the non-equilibrium particles could only be separated

from the thermal particles by means of a parametrization involving two component moving source fits.

The EOS [39] data can be compared with statistical models. There are several statistical models which have been used to study MF, [1,3,4,48–56] but the most widely used are the Statistical Multifragmentation Model (SMM) [3,48–50] and Monte Carlo microcanonical model (MMMC) [1,4]. The theoretical interest in MF is not confined to only statistical models but several other approaches to study MF have been carried out e.g. percolation, lattice gauge and Ising models [22,57–63]. A phenomenological droplet model [64], based on the Fisher [10] droplet model, has also been used to describe the liquid-gas phase transition in nuclear reactions. Here we shall compare the experimental data with the predictions of the SMM model in the manner presented in previous publications [45,47,65,66]. We found that this model is in good agreement with a variety of results for the MF of 1A GeV Au [47]. SMM requires mass, charge and excitation energy of the remnant as input. Using the experimental remnants from Au+C, the parameters of the SMM were fixed based on the agreement between SMM and data. Some comparisons with the data for La+C and Kr+C were also made in later work using the same set of parameters as in case of Au+C [45].

This paper deals with the MF of 1A GeV Au, La, and Kr on carbon. Section II gives a brief summary of the experimental remnant properties. The fragment properties are discussed in Section III. Section IV describes SMM and gives a comparison with the data. The search for the critical transition is discussed in Section V. The determination of various critical exponents is given in Section VI. Energy fluctuations and heat capacity analyses are discussed in Section VII. Section VIII dwells on the nature of the phase transition in Au, La and Kr. Conclusions are given in Section IX.

II. PROPERTIES OF THE REMNANT

The reverse kinematic EOS experiment was performed with 1A GeV ^{197}Au, ^{139}La, and ^{84}Kr beams on carbon targets. The details of the experiment are given in our earlier publica-

tions [39,45]. Only a brief description will be given here. The experiment was done with the EOS Time Projection Chamber (TPC) [67,68] and a multiple sampling ionization chamber (MUSIC II) [69]. The TPC provided almost 4 π solid angle coverage in the center-of-mass system. Three-dimensional tracking and charged particle identification permitted momentum and energy reconstruction of fragments with charges in the range of $1 \leq Z \leq 8$. Particle identification was based on specific energy loss along particle tracks. MUSIC II detected and tracked fragments with charges $8 \leq Z \leq Z_{beam}$. The excellent charge resolution of this detector permitted identification of all detected fragments.

The analysis presented here is based on fully reconstructed MF events for which the total charge of the system was taken as $79 \leq Z \leq 83$, $54 \leq Z \leq 60$, and $33 \leq Z \leq 39$ for Au, La, and Kr, respectively [39,45]. Approximately $\sim$ 32000, 26000, and 42000 events met the above criteria for Au, La and Kr, respectively.

FIGURES

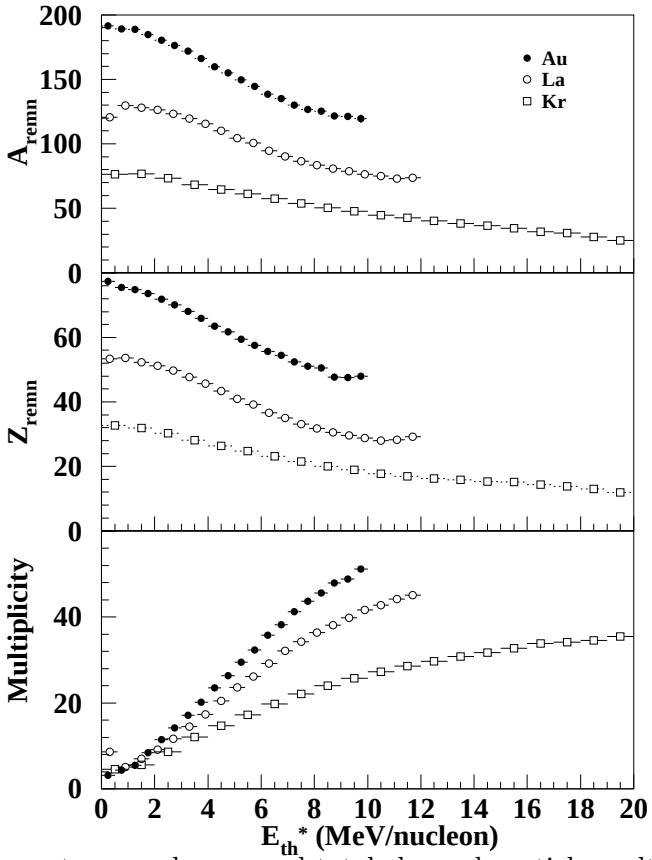

FIG. 1. Average remnant mass, charge, and total charged-particle multiplicity as a function of thermal excitation energy E^*_{th} from the MF of Au, La and Kr.

The remnant refers to the equilibrated nucleus formed after the emission of prompt particles. This remnant then undergoes MF. The charge and mass of the remnant were obtained by removing for each event the total charge of the prompt particles. In order to obtain the mass, the number of prompt neutrons was estimated by means of the ISABEL cascade calculation [70,71]. The excitation energy per nucleon of the remnant, E^*, was based on an energy balance between the excited remnant and the final stage of the fragments [72] for each event, as discussed in detail elsewhere [39,45].

In our previous work we have shown that some of the excitation energy of the remnant includes a nonthermal component which may be ascribable to expansion energy, E_x [39,41,45]. The thermal excitation energy E^*_{th} of the remnants is obtained as the difference between E^* and E_x. This energy is an important quantity both for input to SMM and for the physics

analysis of the data. Fig.1 show plots of A_{remn}, Z_{remn} and total charged particle multiplicity, m, for Au, La, and Kr, respectively, as a function of E^*_{th} [39,45].

The plots in Fig.1 show the nature of the remnant originating from the different system sizes. In case of Au and La one finds that the remnant size at the highest multiplicity is nearly 50% of the initial remnant size, while for Kr the remnant loses up to $\sim$ 70 % of the initial mass. The range of E^*_{th} is also different in the three cases. For Kr the remnant reaches E^*_{th} as high as $\sim$ 20 MeV/nucleon, while for Au and La the maximum E^*_{th} are $\sim$ 9 and $\sim$ 12 MeV/nucleon, respectively. Figure 1 shows the variation of the average m with E^*_{th}, but does not give an indication of event-to-event fluctuations. Fig.2 shows a contour plot of m vs E^*_{th}. These two quantities are fairly closely correlated for Au and La and confirm the linear variation shown in Fig.1. The correlation is much poorer for Kr and a broad range of energies corresponds to a narrow range of m values above 8 MeV/nucleon.

III. FRAGMENT PROPERTIES

We first examine the second stage fragment multiplicities, m_2. Fig.3 shows a plot of m_2 vs E^*_{th} for Au, La, and, Kr. The m_2 for Au and La increase linearly with E^*_{th}, while for Kr m_2 increases slowly up to $E^*_{th}\sim$ 8 MeV/nucleon and remains essentially constant at higher E^*_{th}. The constancy of m_2 above 8 MeV/nucleon suggests that the system may be disintegrating into individual nucleons and light particles, which suggests that the vaporization process becomes dominant. This interpretation is confirmed by the variation with E^*_{th} of the size of the largest fragment, A_{max}, in each event as shown in Fig.4. It is observed for Kr that above $\sim$ 8-9 MeV/nucleon the value of A_{max} is nearly constant with a value of ≤ 6.

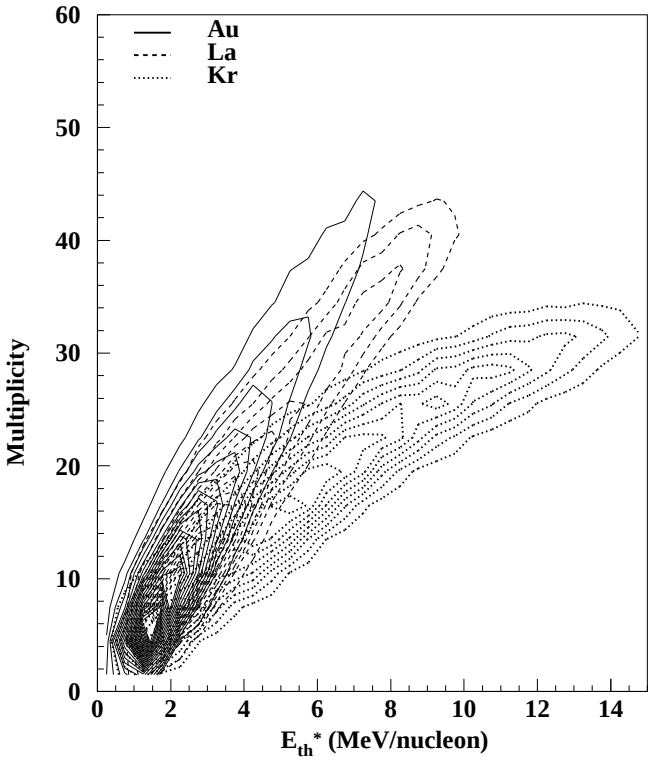

FIG. 2. m as a function of E^*_{th} for Au, La, and, Kr. There are ten equidistant contours.

The distribution of IMFs is shown in Fig.5 for all three systems as a function of energy. In order to exclude fission and/or the largest fragment for all three projctiles we define IMFs as having nuclear charges ranging from Z=3 to Z=$Z_{proj}/4$. Fig.5 shows that for all the three systems the peak in IMFs is $\sim$ 8 MeV/nucleon although the IMF peak for Au is not well defined as $E^*_{th} > 8$ MeV/nucleon was hardly achieved for this projectile. The drop in IMF yields for Au has been seen when the data were plotted as a function of m rather than E^*_{th} because of the dispersion in m values at a given E^*_{th} [45]. Note that the number of IMFs from Kr drops to substantially less than 1 above 10 MeV/nucleon. This is another confirmation of the results given in the preceding section showing the vaporization of the Kr remnants at high E^*_{th}.

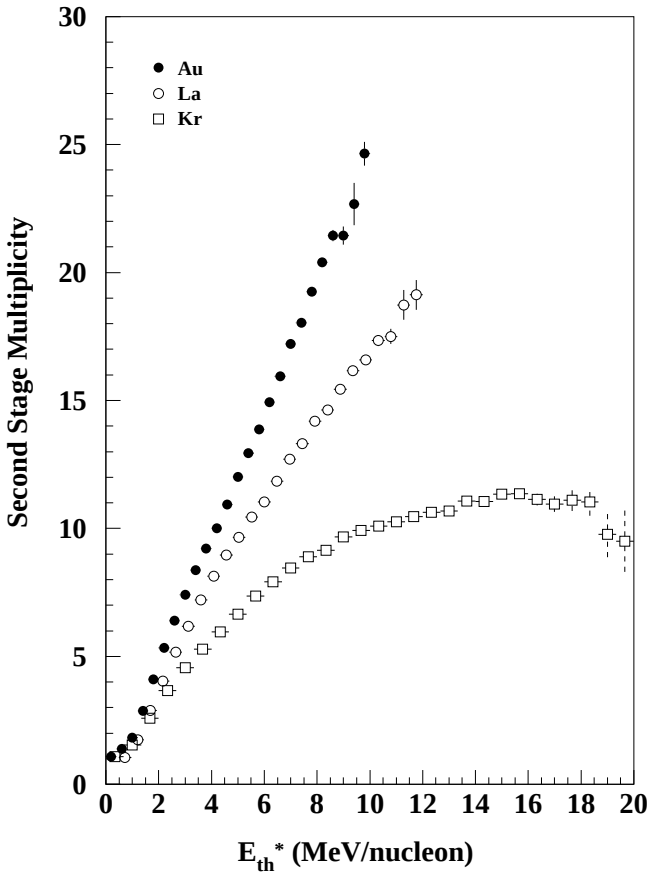

FIG. 3. m_2 as a function of E^*_{th} for Au, La, and, Kr.

IMF production has been studied as a function of projectile bombarding energy by the ALADIN Collaboration [28–30]. They showed that the excitation energy dependence of the average IMF number for Xe, Au, and U projectiles when scaled by charge of the emitting source is similar, suggesting that the IMF production mechanism is independent of the entrance channel. A universal scaling for IMF production has also been seen from a wide range of source masses (35 -190 nucleons) produced in reactions with energies from 35 to 600 MeV/nucleon [73].

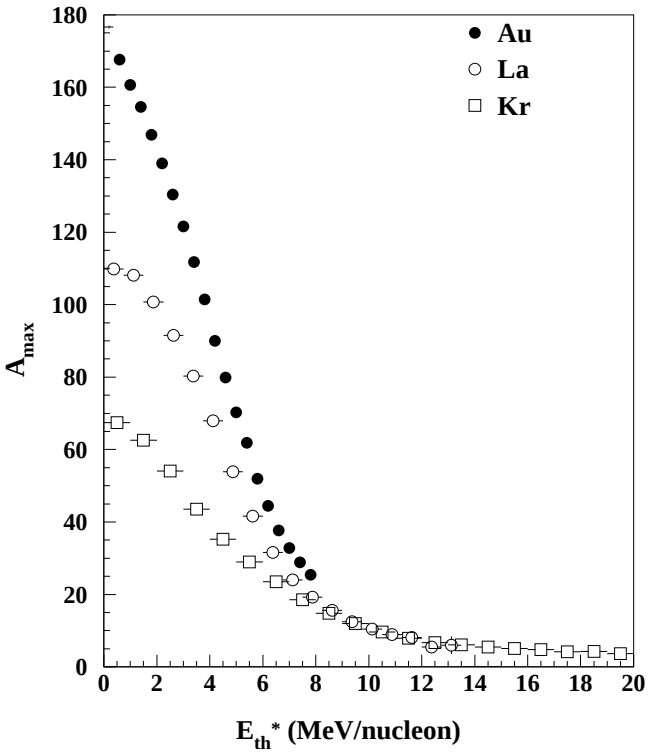

FIG. 4. A_{max} as a function of E^*_{th} for Au, La, and, Kr.

IV. THE SMM MODEL AND COMPARISON WITH DATA

The variable volume version of SMM has been used in this work for comparison with the data. This variable volume corresponds approximately to the condition of constant (close to zero) pressure [74]. SMM is a statistical description of the simultaneous breakup of an expanded excited nucleus into nucleons and hot fragments [3,48,49]. Individual fragments at normal nuclear density are described with a charged liquid drop parameterization. The free energy of a fragment is used to determine the fragment formation probability. This solution explicitly assumes the inhomogeneous nature of the hot MF final state.

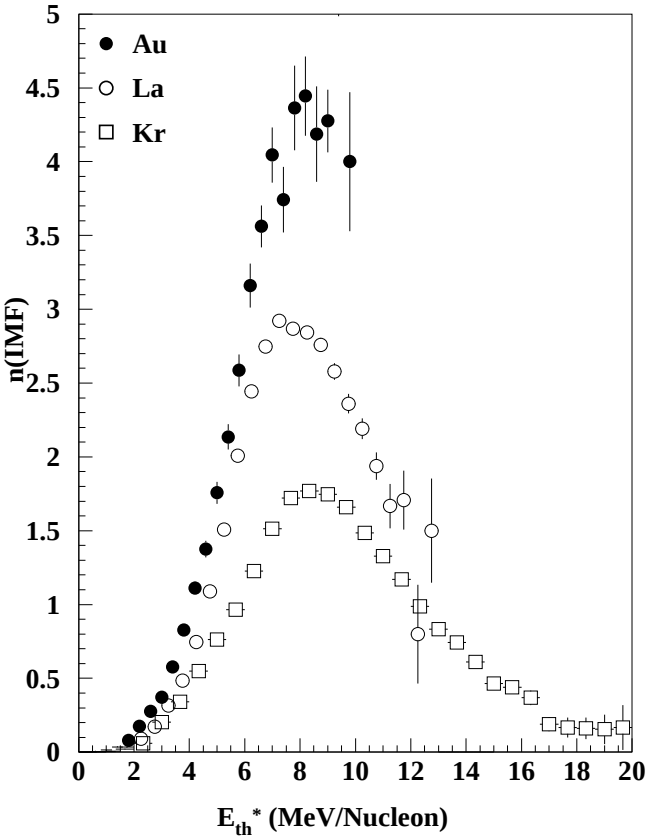

FIG. 5. Average n(IMF) as a function of E^*_{th} for Au, La, and, Kr.

Light fragments with $Z < 3$ may also be present in the hot MF final state. For the $Z \geq 3$ fragments, a quantum mechanical description is used for the temperature dependent volume, surface, and translational free energy of the fragments. The temperature independent parameters are based on the coefficients of the semiempirical mass formula. The critical temperature, at which the surface tension of neutral nuclear matter droplets would go to zero, is in the range suggested by infinite neutral nuclear matter calculations [75].

The two important parameters of the model are the Coulomb reduction parameter, κ, and the inverse level density parameter ϵ_0 [48]. The κ parameter was fixed with the comparison of the measured free volume from SMM to that of the initial volume obtained in the collision process for the Au+C data. The details are given in ref. [47]. The only remaining parameter, ϵ_0, was obtained from the detailed comparison of SMM results with the various experimental fragment properties, e.g. second stage multiplicity, size of the biggest fragment, and IMFs

using Au+C data [47]. In this work the same value of κ=2 and ϵ_0=16 MeV has been used in SMM to compare results with data for La and Kr. The best agreement with the data was found by using the standard values of the parameters of the model.

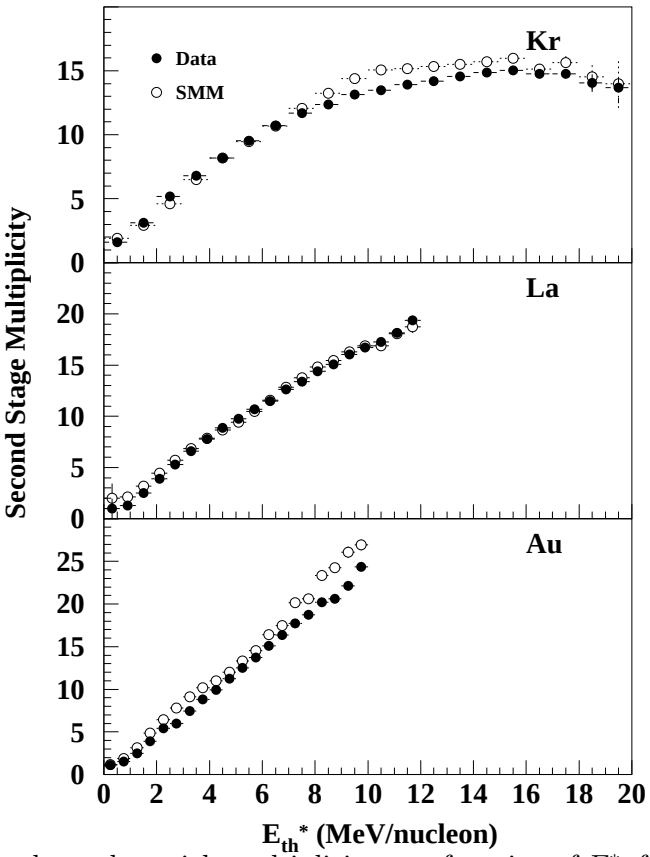

FIG. 6. Second stage charged-particle multiplicity as a function of E^*_{th} for Kr, La, and, Au from data and SMM.

The SMM results were also compared with the data on La and Kr [45], with the same parameters as in Au, using reduced multiplicity (m/Z_{proj}). Here we present a few comparisons between data and SMM using E^*_{th}. Fig.6 shows a plot of m_2 as a function of E^*_{th} for Au, La and Kr. The agreement between data and SMM is very good. The flatness of m_2 beyond $E^*_{th}\sim$ 8 MeV/nucleon observed for Kr is also seen in SMM. The size of the largest fragment from both data and SMM is shown in Fig.7 for all the three systems. Very good agreement between the two is obtained over the entire range of E^*_{th}.

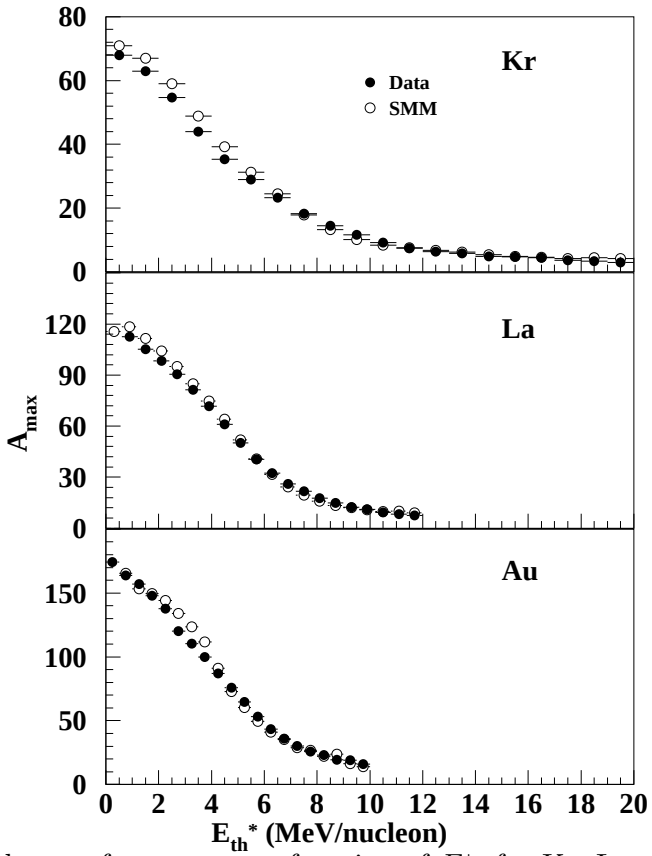

FIG. 7. Size of the largest fragment as a function of E^*_{th} for Kr, La, and, Au from data and SMM.

The average value of the total number of IMFs as a function of E^*_{th} is shown in Fig.8 for both data and SMM. Both show the same initial increase in IMF production and a peak at approximately the same energy. SMM follows the trend in the Kr data in the vaporization regime, where the IMF multiplicity decreases to zero at the highest energy. SMM overestimates the number of IMF at the peak in all three cases. This difference is due to the fact that in SMM there is overproduction of Li and Be fragments at higher excitation energies.

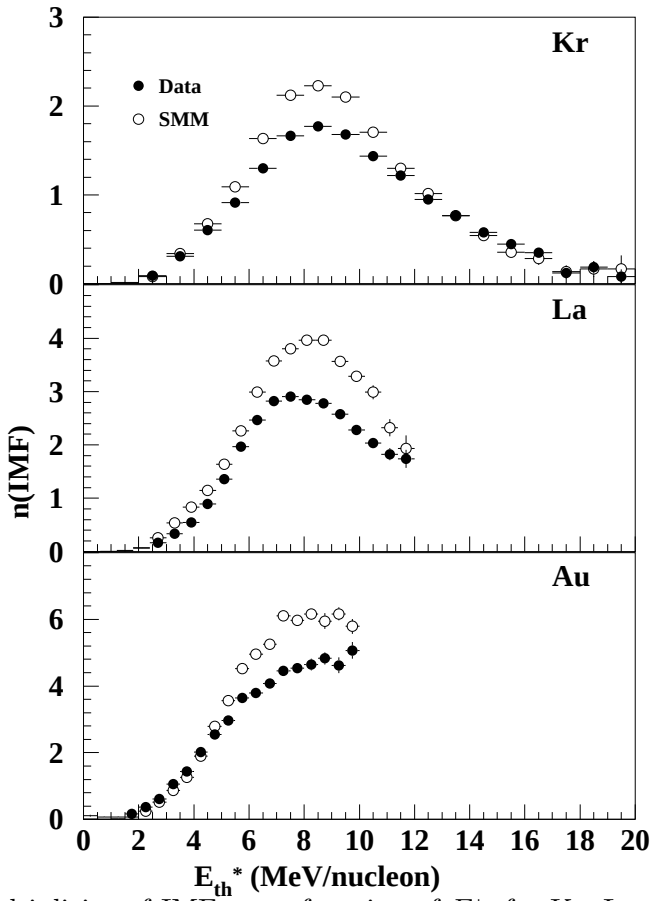

FIG. 8. Average multiplicity of IMFs as a function of E^*_{th} for Kr, La, and, Au from data and SMM.

The above comparison between data and SMM was done with SMM calculations including the deexcitation of secondary fragments. SMM can also be stopped prior to secondary decay to obtain information about the SMM primary fragments. We refer to these results as SMM_{hot} while those following secondary decay are designated SMM_{cold}. As will be seen in the following sections SMM_{hot} can be used to evaluate the nature of the phase transition. A full description of SMM_{hot} for the remnant system with A=160 and Z=64 has been given in ref. [47].

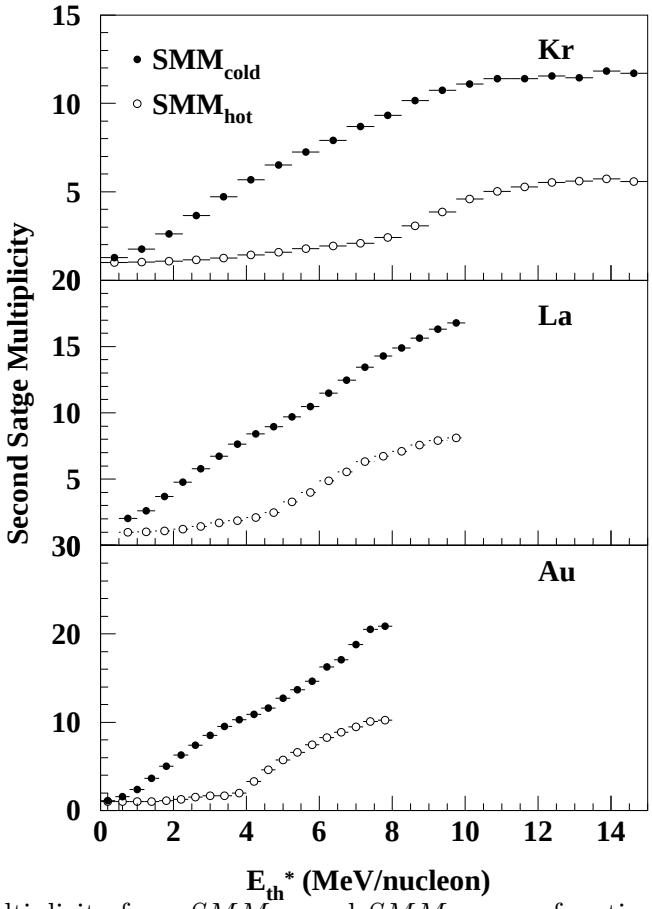

FIG. 9. Average multiplicity from SMM_{hot} and SMM_{cold} as a function of E^*_{th} for Kr, La, and, Au.

The m_2 distributions as a function of E^*_{th} for both SMM_{cold} and SMM_{hot} are shown in Fig.9. There is an increase in multiplicity for SMM_{cold} in all three cases. For SMM_{hot} m_2 remains nearly unchanged up to a certain energy and then suddenly increases. The energy at which m_2 starts increasing corresponds to the MF threshold. The values of E^*_{th} at which MF first occurs are ~ 4, ~ 5, and ~ 8 MeV/nucleon for Au, La and Kr, respectively. The threshold energy is lowest for the heaviest system because of the large Coulomb energy in the heavier remnant, which facilitates the breakup of the nucleus at a lower energy. There is a very narrow window for Kr between the multifragmentation threshold and the energy at which vaporization starts. This reduces the probability of IMF formation, as is evident from Fig.5.

V. CRITICAL POINT DETERMINATION

In our earlier publications we discussed the 1A GeV Au on carbon data in terms of the theory of critical phenomena and several critical exponents were determined [36,38,40,43,44]. We used the percolation technique applied to small lattices to study critical phenomena [76,77,35]. The method of moments analysis was used by several groups [29,57,78–82] to search for evidence of the liquid-gas phase transition in MF. Recently, we used this method in the analysis of La and Kr data [46] using charged particle multiplicity as the order parameter. In this work E^*_{th} is used as the order parameter. E^*_{th} is a more fundamental parameter than multiplicity for comparing the three systems. Here, we first use the combination of moments to find the signature of criticality in Au, La and Kr data. For example, the reduced variance $\gamma_2 = M_2 M_0 / M_1^2$, where M_1 and M_2 are the first and second moments of the mass distribution in an event and M_0 is the total multiplicity including neutrons, is a useful quantity. The reduced variance γ_2 has a peak value of 2 for a pure exponential distribution, $n_A \sim e^{-\alpha A}$, regardless of the value of α, but $\gamma_2 > 2$ for a power law distribution, $n_A \sim A^{-\tau}$, when $\tau > 2$ and the system is large enough. Critical behavior requires that the peak value of γ_2 be larger than 2 [21,22].

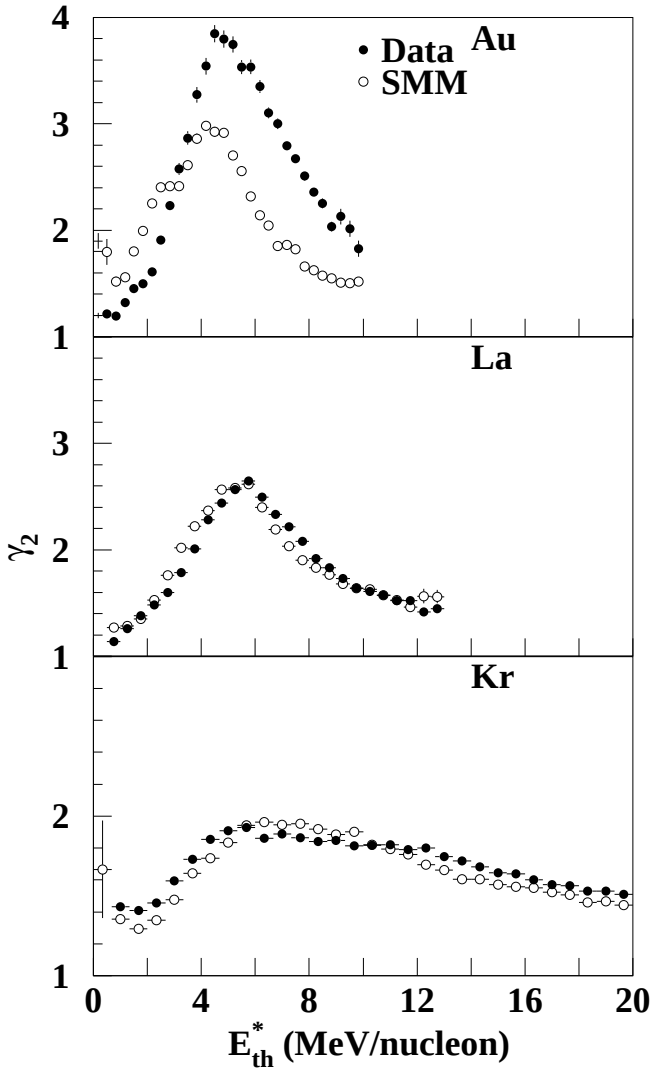

FIG. 10. γ_2 as a function of E^*_{th} for all the three systems from data and SMM_{cold}.

The event by event analysis for γ_2 is shown in Fig.10 for all the three systems. The position of the maximum γ_2 value defines the critical point, *i.e.* the critical energy E^*_c, where the fluctuations in fragment sizes are the largest. The peak in γ_2 is well defined for La and Au. The value for E^*_c is in good agreement with our earlier values, where m_c was used as the order parameter and E^*_c was obtained from E^*_{th} vs m plot [46]. In case of Kr Fig.10 shows that there is no well defined peak in γ_2 and the distribution is very broad. A well defined peak is obtained in m_c, but the value of γ_2 is always less than 2 [46].

Fig.10 also shows the γ_2 calculation using SMM_{cold}. The fission contribution to γ_2 has been removed both from the data analysis and SMM. The E^*_c values obtained for data and

SMM_{cold} are close to each other. There is a difference in the height of the peak in γ_2 for Au between data and SMM_{cold}. It is also important to note that at the peak $\gamma_2 > 2$ both from SMM_{cold} and data for Au and La and $\gamma_2 < 2$ for Kr. This suggests that the exponent $\tau < 2$ for Kr as there is no enhancement of γ_2 in the critical region . One expects an enhancement of the moments in the critical region with $\tau > 2$ as in most critical phenomena [26,27].

In case of Au the γ_2 value remains above two for most of the excitation energy range. The E^*_{th} width over which $\gamma_2 > 2$ is smaller for La and disappears for Kr. The decrease in γ_2 with decrease in system size, as observed in Fig.10, is also seen in 3D percolation studies and the differences have been attributed to finite size effects [83,84]. The results for E^*_c are given in Table I along with the values of m_c [46].

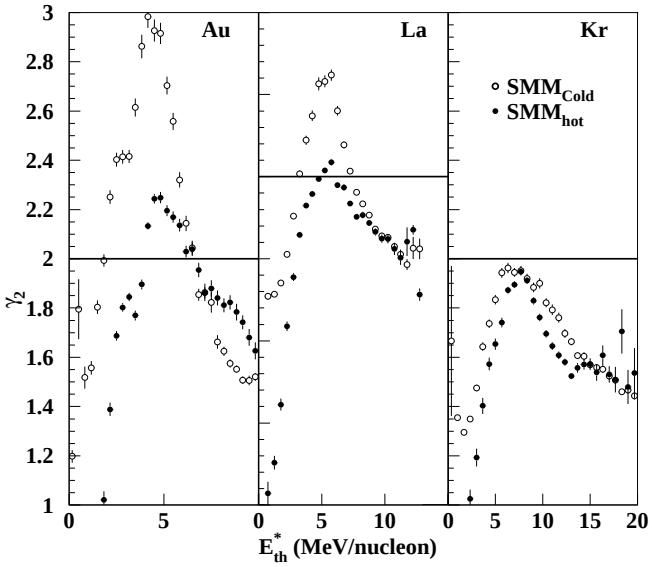

FIG. 11. γ_2 as a function of E^*_{th} from SMM_{hot} and SMM_{cold}

It is of interest to see how the critical point determination from SMM_{hot} compares with that of SMM_{cold}. Since SMM_{cold} can reproduce the various features of the EOS data, one can use SMM_{hot} to understand the MF mechanism. Fig. 11 shows a plot of γ_2 as function of E^*_{th} from SMM_{cold} and SMM_{hot}. It is evident from the plots for Au and La that the peak in γ_2 occurs at the same E^*_{th} for both SMM_{cold} and SMM_{hot}. The distinct difference is in the height of the peak. For SMM_{hot} the height of the γ_2 peak is smaller as compared to SMM_{cold}, but still above 2. This difference is mainly due to the increase in SMM_{cold}

multiplicity as compared to SMM_{hot}. In the case of Kr the γ_2 value is always less than 2 for both SMM_{cold} and SMM_{hot} and the height of the γ_2 peak does not decrease from SMM_{cold} to SMM_{hot} as for Au and La. A detailed calculation of critical exponents from SMM_{hot} has been given in our earlier publication [47]. These results clearly demonstrate that SMM_{hot} and SMM_{cold} behave in a similar way. The most important conclusion is that the values of the exponents do not change in going from SMM_{hot} to SMM_{cold}. Thus, SMM_{hot} results are consistent with a critical phase transition for Au and La and not for Kr.

VI. CRITICAL EXPONENTS ANALYSIS

A. τ Exponent

In the previous section it was shown, based on the γ_2 analysis, that Au and La should show a power law with exponent $\tau \geq 2$ for a continuous phase transition to be present. τ can be obtained using the moments of the fragment mass distributions.

Scaling theory [26] relates the values of the critical exponents τ and σ to the moments M_k of the mass distribution through

$$M_k \propto |p - p_c|^{-(1+k-\tau)/\sigma} \tag{1}$$

where p is the bond breaking probability and at the critical point p=p_c in percolation. The values of τ and σ in the above equation are characteristic for the specific class of phase transition. For a transition of the 3D percolation type $\tau = 2.2$ and $\sigma = 0.45$, while for a liquid-gas phase transition a value of $\tau = 7/3$ and $\sigma = 2/3$. The 3D Ising values for τ and σ are 2.2 and 0.64 respectively. The τ value is essentially the same for different universality classes. The above equation can be solved to get the value of τ if the second (M_2) and third moments (M_3) of the fragment mass distributions are known. A plot of $ln(M_3)$ versus $ln(M_2)$ should give a straight line with a slope given by

$$S = \frac{\Delta ln(M_3)}{\Delta ln(M_2)} = \frac{\tau - 4}{\tau - 3} \tag{2}$$

Fig.12 shows a scatter plot of $ln(M_3)$ vs $ln(M_2)$ for all the three systems from data above E_c^* [76]. Also shown in Fig.12 are the results from SMM_{cold}. A linear fit to $ln(M_3)$ vs $ln(M_2)$ gives the value of τ. The τ values are shown in Table I both from data and SMM. A linear fit to the Kr data gives a value of $\tau = 1.88 \pm 0.08$. This value is below the minimum value $\tau \geq 2$ expected for a continuous phase transition. This result for Kr is consistent with Fig.10, which shows that $\gamma_2 < 2$ and hence $\tau < 2$ [21,22]. Similar results are also obtained for SMM_{cold}.

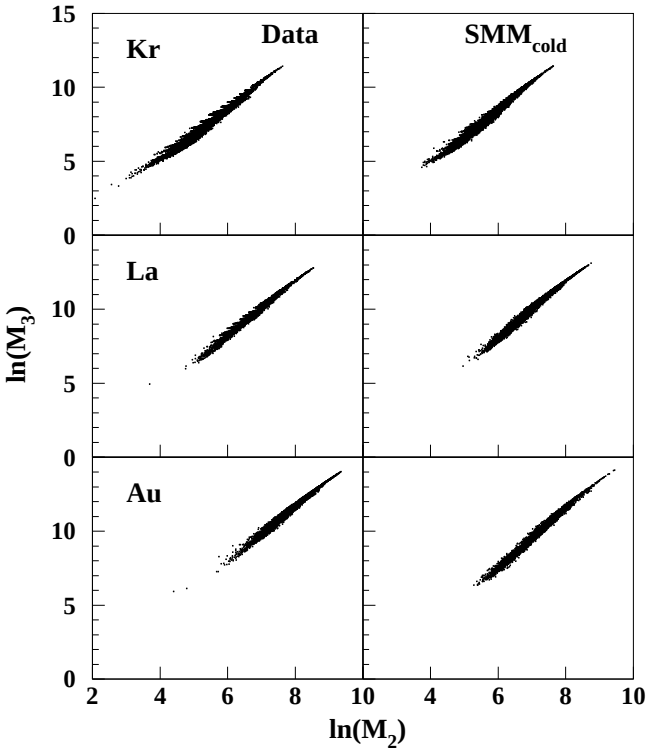

FIG. 12. $ln(M_3)$ vs $ln(M_2)$ for Au, La and Kr above the critical energy.

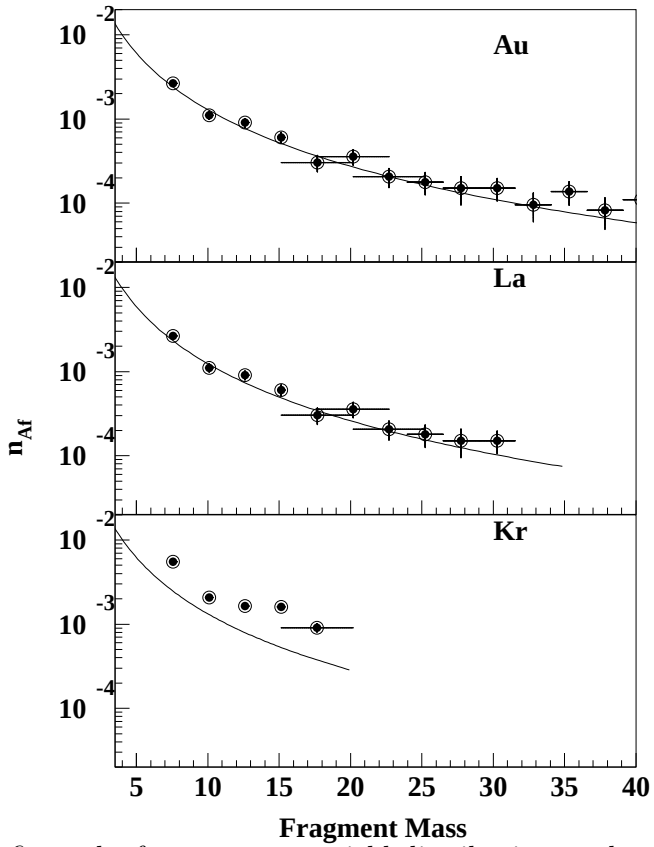

FIG. 13. Power law fit to the fragment mass yield distribution at the critical point. The solid line corresponds to $n_{Af} \sim q_0 A^{-\tau}$, with q_0=0.2 and τ=2.2[43].

TABLES

TABLE I. Critical parameters from data and SMM_{cold}

Parameter	Au_{data}	La_{data}	Kr_{data}	Au_{smm}	La_{smm}	Kr_{smm}	Per[a]	LG[b]
m_c	28±3	24±3	18±2	26±3	23±3	17±2		
E_c^*	4.5±0.5	5.5±0.6	6.5±1.0	4.3±0.5	5.3±0.6	6.2±1.0		
τ	2.16±0.08	2.10±0.06	1.88±0.08	2.11±0.05	2.05±0.05	1.81±0.06	2.20	2.21
β	0.32±0.02	0.34±0.02	0.53±0.05	0.35±0.03	0.37±0.03	0.57±0.06	0.44	0.328
β/γ	0.22±0.03	0.25±0.01	0.50±0.01	0.28±0.03	0.29±0.05	0.52±0.01		
γ	1.4±0.3[c]	-	-	1.02±0.23[c]	-	-	1.76	1.24
γ	1.32±0.15[d]	1.20±0.08[d]						

a. Percolation, b. Liquid-Gas, c. ref.[47], d. from β and β/γ ratio

A one-parameter power law search also provides an alternative method for the determination of τ [43]. At the critical point the cluster distributions were described by $n_{Af} \sim q_0 A^{-\tau}$ with $\tau \sim 2.2$ and $q_0 \sim 0.2$, as seen in many universality classes [43]. Fig.13 shows a plot of the fragment mass distribution at the critical energy for Au, La and Kr. The line corresponds to $n_{Af} = q_0 A^{-\tau}$ with τ=2.2 and q_0=0.2 [43]. It is clear from the plot that Kr data do not follow the above power law with the critical values of q_0 and τ.

B. β exponent

Using the methods developed in percolation studies the value of the exponent β can be obtained for the MF of 1A GeV Au+C [36]. It is related to the size of the largest cluster by the relation

$$A_{max} \sim |\epsilon|^{\beta} \tag{3}$$

where $\epsilon = p - p_c$ and $\epsilon > 0$. In the MF case p and p_c have been replaced by E^*_{th} and E^*_c. In the infinite lattice, the infinite cluster exists only on the liquid side of p_c. In a finite lattice a largest cluster is present on both sides of the critical point, but the above equation holds only on the liquid side. When $\epsilon < 0$, no infinite cluster exists and the size of the finite cluster is given by

$$A \sim |\epsilon|^{-(\beta+\gamma)} \tag{4}$$

where γ is another critical exponent and related to the second moment, M_2

$$M_2 \sim |\epsilon|^{-\gamma} \tag{5}$$

Fig.14 shows a plot of $ln(A_{max})$ vs $E^*_{th} - E^*_c$ from Au, La and Kr. The values of β obtained from the fit are given in Table I. The values of β for Au and La are 0.32±0.02 and 0.34±0.02, respectively, and close to the value of 0.33 predicted for a liquid-gas phase transition. The value of β for Au is in agreement with our earlier reported value [36]. In

case of La β is close to the value obtained for Au, while the value of β= 0.53±0.05 for Kr is much higher than that of Au and La.

It is interesting to note that the SMM calculation also gives the same results as obtained in data. Fig.14 shows results from SMM as open circles for all the three systems. These comparisons with SMM are important, as this will help us to probe the order of phase transition using SMM in the three experimentally studied systems.

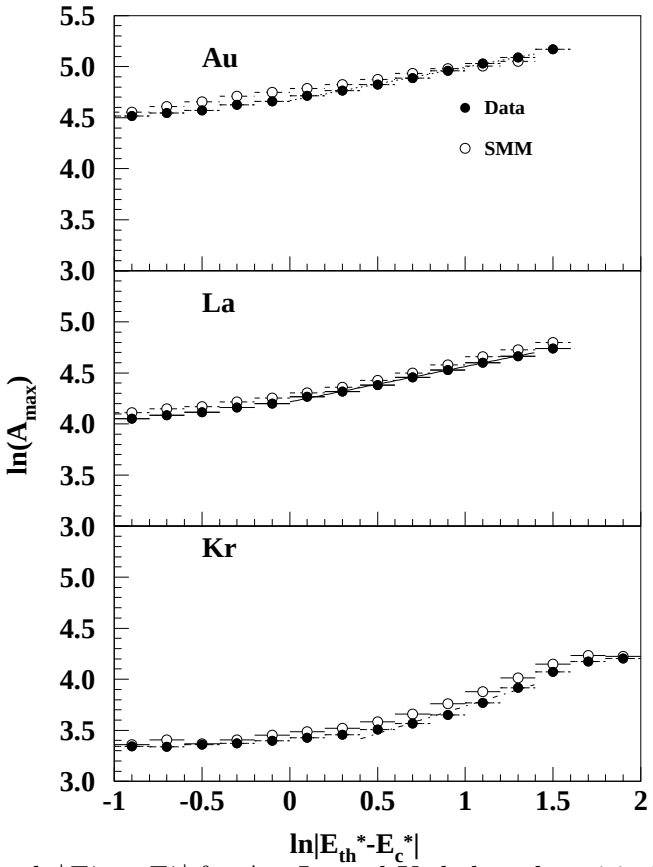

FIG. 14. $ln(A_{max})$ vs $ln|E^*_{th} - E^*_c|$ for Au, La and Kr below the critical energy for exponent β determination.

Campi [21,22] also suggested that the correlation between the size of biggest fragment, A_{max}, and the moments in each event can measure the critical behavior in nuclei. Fig.15 shows a plot of the logarithm of A_{max} in each event versus the logarithm of the second moment M_2 for all the three systems. This plot is generally called a Campi scatter plot and has been successfully used in many studies [85,86]. The two branches corresponding to the under-critical (upper branch) and over-critical (lower branch) events are clearly seen for

Au and La. The A_{max} - M_2 correlation is quite broad for Kr and fills most of the available phase space. The lower and upper branches seems to overlap and are not well separated. Studies on percolation lattices show similar behavior [85]. However, it is not possible from such a plot to locate the critical region in a precise and unambiguous manner. But, if we know the critical point from some other method, then the A_{max}- M_2 correlation can be used to calculate the ratio of critical exponents β/γ from the slope of the upper branch. A similar behavior is obtained from SMM as shown in Fig. 15 for all the three systems.

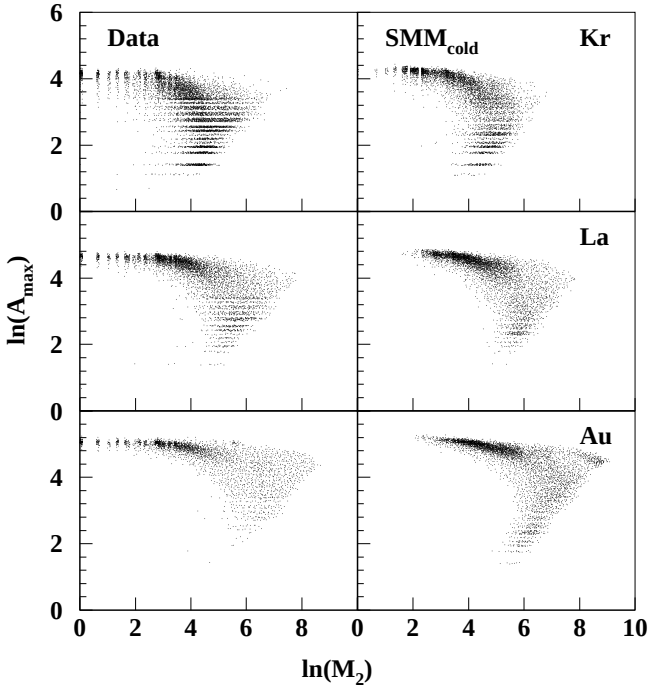

FIG. 15. Scatter plot of the $ln(A_{max})$ vs $ln(M_2)$ from data and SMM_{cold}.

Table I shows the β/γ values for Au and La from the linear fit to the upper branch of Fig.15. For the fitting purpose an average value of $ln(A_{max})$ was obtain for each value of $ln(M_2)$.

We have mentioned only a few exponents in this analysis and compared them with SMM. The aim is to show that Kr is different than Au and La. The two exponents τ and β serve this purpose very well. Knowing β and β/γ, γ can be obtained. Results are listed in Table I and the value for Au agrees with the published value. Table I also gives the values of the critical exponents for the percolation and liquid-gas phase transition in 3D systems. No

attempt has been made in this paper to independently determine other exponents like γ and σ. All the exponents for Au and their comparison with SMM have been reported in various publications [36,38,40,47].

VII. ENERGY FLUCTUATIONS AND HEAT CAPACITY ANALYSIS

In a recent study experimental evidence of a liquid-gas phase transition in MF was offered by analyzing the fluctuations in the total fragment energy [92,93]. It has been shown that for a given total energy the average partial energy stored in a part of the microcanonical system is a good thermometer while the fluctuations associated with the partial energy can be used to determine the heat capacity, which is negative for a first order transition and positive for a second order transition.

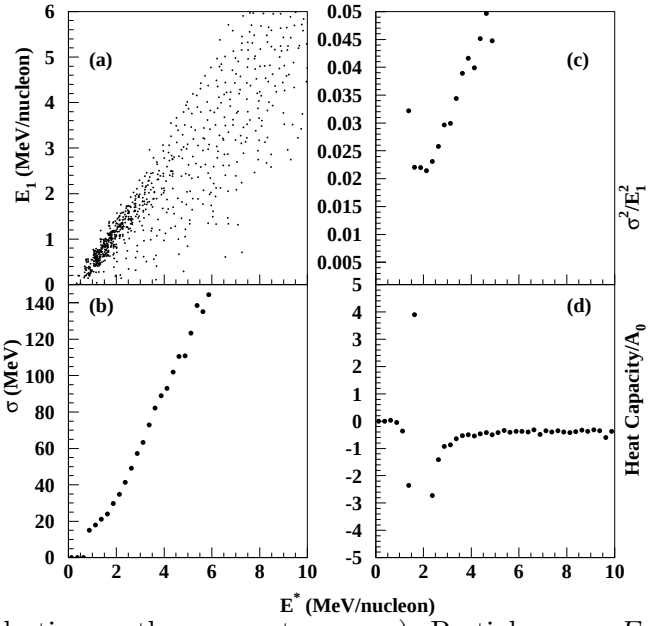

FIG. 16. With no selection on the remnant mass: a). Partial energy E_1 as a function of E^* b). Fluctuation in E_1 c). The variance $(\sigma/E_1)^2$ and d). Heat capacity per nucleon for Au .

A negative heat capacity was obtained in the reaction Au+Au at 35A MeV, providing the direct evidence of a first order liquid-gas phase transition [93]. We have analyzed our data for Au and Kr using energy fluctuations. From the total excitation energy E^* the Coulomb and expansion energy components were removed to obtain energy E_1 [39,45].

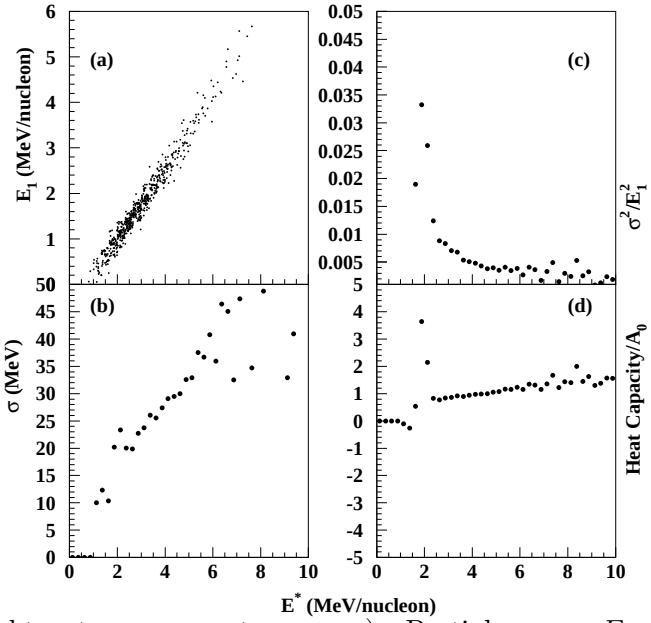

FIG. 17. With a tight cut on remnant mass: a). Partial energy E_1 as a function of E^* b). Fluctuation in E_1 c). The variance $(\sigma/E_1)^2$ and d). Heat capacity per nucleon for Au.

The fluctuations in E_1 were studied as a function of E^*. Figs. 16(a) and (b) show the spread in E_1 and its standard deviation σ respectively, as a function of E^*. The reduced variance $(\sigma/E_1)^2$ is shown in Fig. 16(c). The heat capacity C_t is given by

$$C_t = C_1^2/[C_1 - (\sigma/T)^2] \tag{6}$$

where C_1 is the canonical specific heat. It was argued that a negative C_t in the critical region is a signature of a first order phase transition [92,93]. In Fig. 16(d) C_t is shown as a function of E^*. There is a negative heat capacity at $E^* \sim$ 2-3 MeV/nucleon.

However, a different result is obtained if there is a selection on the remnant mass. Figs. 16(a) and (b) have no remnant mass cut and the average mass is 170 ± 19. This causes large fluctuations in E_1. Figs. 17(a)-(d) show similar plots as in Figs. 16(a)-(d) with the remnant restricted to 161 ± 3. Two important results come out of these plots. First, σ is much smaller when the remnant mass cut is applied. Second, C_t is always positive. Our analysis for Au data shows no negative heat capacity. Based on our statistical and thermodynamic analysis, we see indications for a continuous phase transition in Au data [36,38,40,47]. The results for La are similar to those shown above for Au.

A similar analysis was performed on Kr data and results are shown in Figs. 18(a)-(d) and Figs. 19(a)-(d) for remnant masses 58 ± 14 and 56 ± 3 respectively. We do not see the signature of a first order transition even in Kr if the remnant mass is selected in a narrow bin. On the other hand a negative value of C_t is obtained if there is no selection on the remnant mass.

Here, we emphasize again that the event-by-event complete reconstruction of remnant mass and excitation energy is very important for the above analysis. This is possible only in high energy reverse kinematic asymmetric collisions [39]. In case of the EOS data, though there is a positive specific heat, there are no large scale fluctuations in it to define the critical energy. Only Au has a peak in C_t, which is around 2-3 MeV/A. There is no peak in C_t for La and Kr. Thus the analysis of EOS data for all three systems based on heat capacity is questionable.

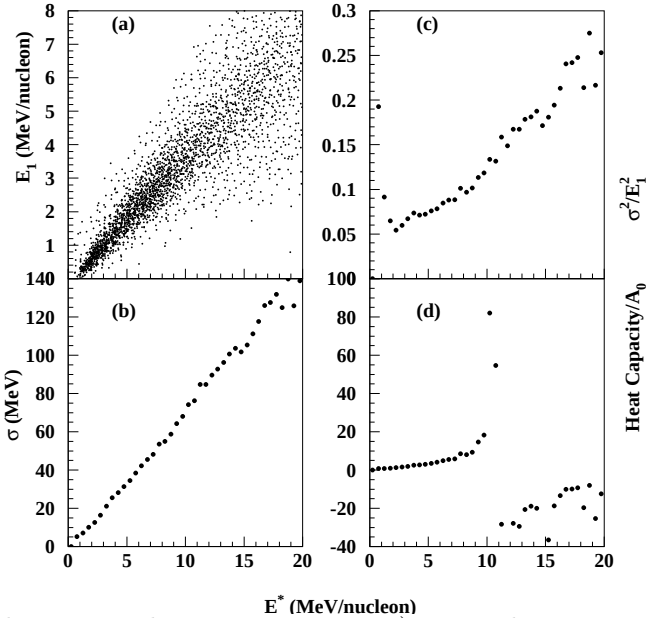

FIG. 18. With no selection on the remnant mass: a). Partial energy E_1 as a function of E^* b). Fluctuation in E_1 c). The variance $(\sigma/E_1)^2$ and d). Heat capacity per nucleon for Kr

VIII. NATURE OF PHASE TRANSITION

In the previous sections we have shown that the MF of Kr is different than that of Au and La. Based on the experimental results it is not possible to decide the order of phase transition in Kr. The statistical analysis suggests a continuous phase transition for Au and La.

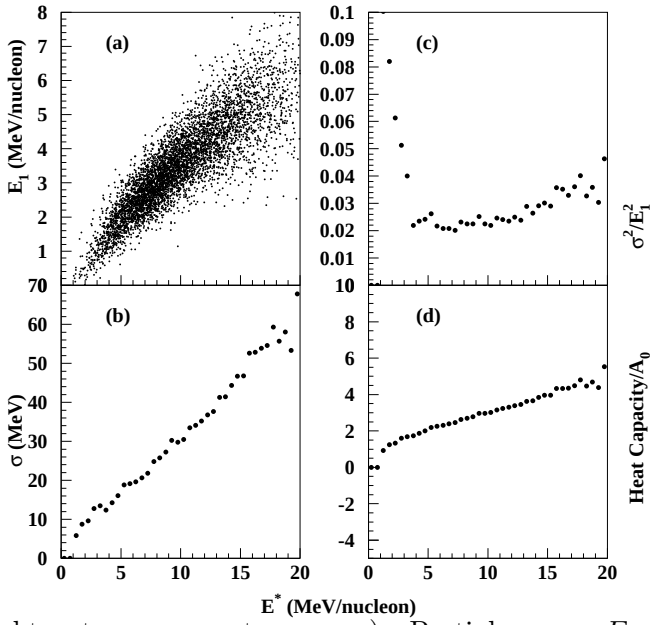

FIG. 19. With a tight cut on remnant mass: a). Partial energy E_1 as a function of E^* b). Fluctuation in E_1 c).The variance $(\sigma/E_1)^2$ and d). Heat capacity per nucleon for Kr

In our earlier publication [47] and in this paper as well we have shown that SMM can reproduce the various features of EOS data, including the critical exponents. A single set of parameters of the model was used to describe the data for all the three systems, Au, La, and Kr. The nature of the phase transition in SMM was analyzed using SMM_{hot}, i.e. fragments formed before secondary decay [47]. The microcanonical temperature was obtained for the MF system and a caloric curve was constructed [1,47,94] for A=160, 130, 100, and A=70. A backbending in the caloric curve is an indication of a first order phase transition and leads to a negative specific heat. For A=160 there is a positive peak in the specific heat vs energy plot, consistent with our energy fluctuation analysis on our data, using a mass cut.

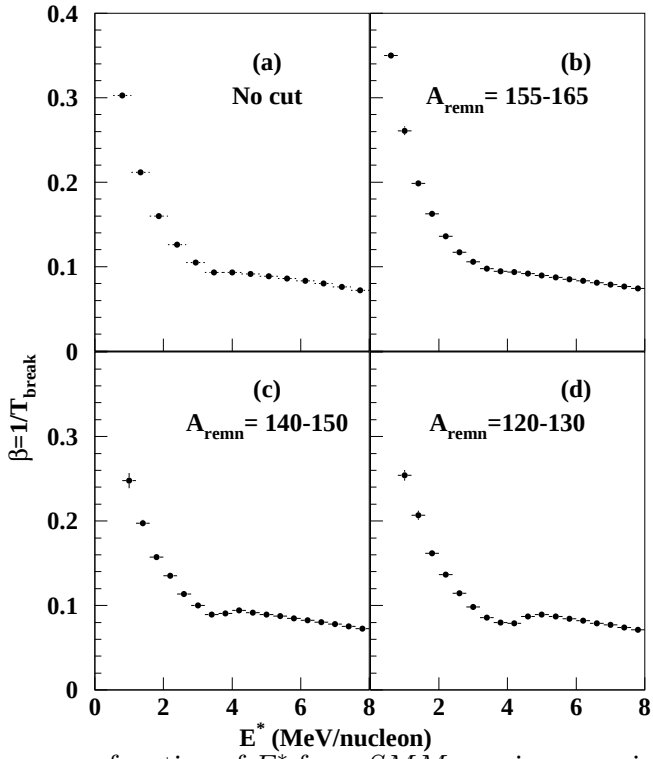

FIG. 20. $\beta = 1/T_{break}$ as a function of E^* from SMM_{hot} using experimental remnant as input to SMM. The graphs are shown for different mass selection on the remnants from MF of Au.

The back-bending in the caloric curve is sensitive to the remnant mass. We have used the remnant distributions from Au+C and Kr+C data to study the remnant mass effect on the caloric curve. Figs.20(a)-(d) show a plot of the reciprocal of the SMM_{hot} breakup temperature $\beta = 1/T_{break}$, for Au. A distinct pattern is evident. A small back bending starts appearing at the very low mass cut. For heavier masses there is no back-bending. Since the remnant mass distribution from Au+C interaction is dominated by heavier remnants, the effect of lighter remnants on back-bending is almost negligible. Fig.20 suggests that, according to SMM, the MF transition in Au changes from first order to second order depending on the remnant mass. For Kr, the back-bending is very sensitive to the particular mass cut. If there is no selection on mass cut the caloric curve is different than those with mass cuts as shown in Figs. 21(a)-(d). However, back-bending is always present. Thus, based on the above reasoning we can say that in case of Kr there is no continuous phase transition. Rather, analysis of the caloric curve argues for a first order phase transition in Kr.

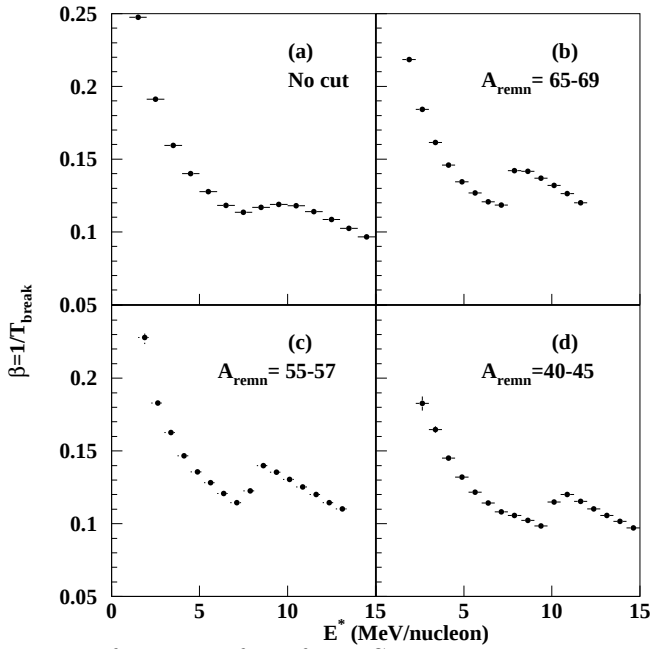

FIG. 21. $\beta = 1/T_{break}$ as a function of E^* from SMM_{hot} using experimental remnant as input to SMM. The graphs are shown for different mass selection on the remnants from MF of Kr.

So far we have shown that the Kr data are different than the Au and La data. The temperature of the MF system provides further insight. One can obtain the freeze out temperature of the cold fragments in data using the ratio of light fragment isotopic yields [39,45,96]. In Fig.22(a) the isotope ratio temperature (T_{He-DT}), as obtained from $^2H/^3H$ to $^3He/^4He$ yield ratio at the critical point E^*_c, is shown for Au, La and Kr systems as function of the linear size of the system (L= $A^{1/3}_{remn}$).

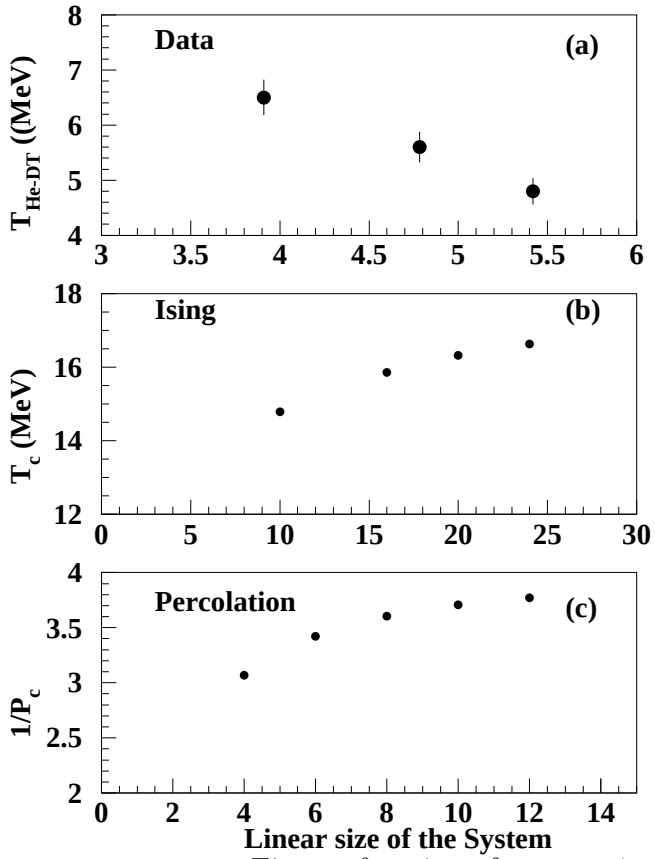

FIG. 22. a). T_{He-DT} temperature at E_c^* as a function of system size from data b). Critical temperature from Ising model calculation and c). Critical bond formation probability plotted as $1/p_c$ for different lattice sizes.

T_{He-DT} decreases with an increase in system size. Recently, in an another study it has also been shown that critical temperatures and excitation energies decrease with increasing system size [95]. This result can be attributed to the higher Coulomb energy in Au as compared to Kr, which in turn shifts the MF transition to lower temperature. The behavior of T_{He-DT} with system size is different than those observed either in percolation or Ising model studies. Fig. 22(b) shows a plot of the critical temperature from a 3D Ising-type model with fixed density [62] for different lattice sizes. In the Ising calculation the trend is different than the one observed in Fig. 22(a). Thus, for neutral matter the critical temperature increases with an increase in system size. We can also compare the results from data and the Ising model calculation with percolation studies. In percolation the critical probability p_c in bond building percolation decreases with increase in the system size [77,97]. Fig. 22(c) shows

$1/\ p_c$ vs percolation lattice size, where p_c is inversely proportional to T_c [97]. Thus, MF of Au, La and Kr is different than 3D Ising and percolation models. As mentioned earlier, the finite size affects only non-thermodynamical quantities e.g. γ_2, A_{max}, etc. and not energy or temperature.

The critical energy is shown in Fig.23(a) as a function of system size. The decrease in E_c^* with increase in system size is evident from the figure. SMM also predicts the critical energy of the MF transition and this energy is shown in Fig.23(a) along with the data. This energy is obtained at the hot fragment stage from the peak in γ_2 as shown in Fig.11. Both data and SMM E_c^* are in good agreement. The breakup temperature T_{SMM}, as obtained from SMM_{hot}, along with the T_{He-DT} from data is shown in Fig.23(b). There is a decrease in both temperatures with increase in system size. It is apparent that T_{He-DT} is about 1 MeV lower than the SMM temperature. This difference is due to the fact that T_{He-DT} is measured after secondary decay has taken place, while T_{SMM} corresponds to the breakup configuration. Note that T_{He-DT} tracks T_{SMM} with system size at the critical point. SMM indicates that the decrease in both T_{SMM} and E_c^* with increasing system size is due to the increase of Coulomb energy. This result suggests that Coulomb energy plays an important role in the MF of nuclei. It is interesting to note that the critical energy obtained both from SMM and data corresponds to the MF threshold as shown in Fig.9. The significance of this result remains to be determined.

The effects of finite size and Coulomb force on the MF have been studied by several workers and it is found that the decrease in critical temperature with increase in system size is primarily due to the Coulomb energy [98–100]. The result from one such calculation is shown Fig.23(b) as T_{limit} [100].

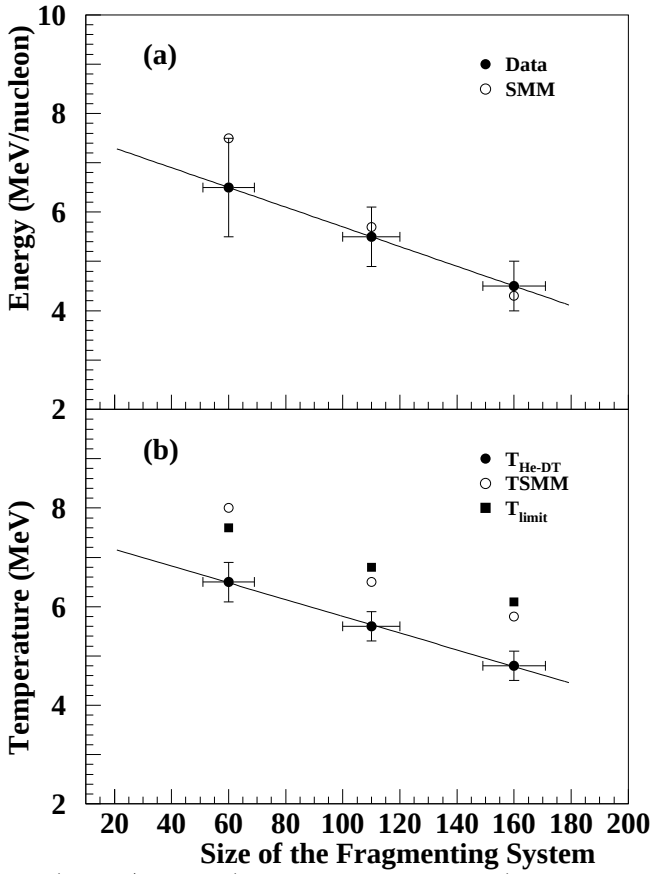

FIG. 23. a). Energy (MeV/nucleon) at critical point. b). T_{He-DT}, T_{SMM} and T_{limit} as a function of the system size.

The microcanonical Metropolis Monte Carlo (MMMC) [1,4] calculations have emphasized that MF is controlled by the competition between long range Coulomb forces and finite size effects (especially surface energy). Finite size effects in models with only short range forces predict an increase in the critical temperature as the system size increases, as is evident from percolation [97] and Ising model studies [62] (see Fig.22). Since the experimental temperature exhibits the opposite dependence on system size, it is apparent that Coulomb effects are more important than finite size effects. For finite *neutral* matter the critical temperature (T_c) is expected to be $\sim$ 15-20 MeV [98,101]. The observed T_c for A=160 is $\sim$ 6 MeV. Compared to finite uncharged nuclei, the presence of Coulomb energy plays a role in lowering the excitation energy needed to reach the regime where critical signatures are observed. In the smaller Kr system there is less Coulomb energy in the initial remnant state. Achieving

multifragmentation in this system requires greater excitation energy/nucleon compared to Au and La (as shown in Fig. 23(a)) and as a result, the dynamics of the ensuing disassembly may not take this system near its critical regime.

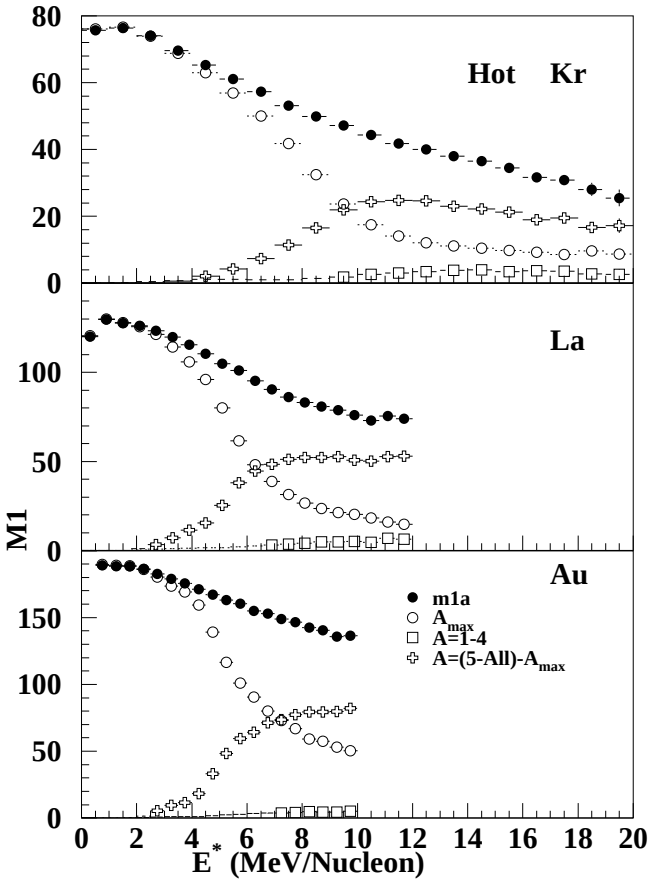

FIG. 24. M1 distribution for SMM_{hot} for Au, La and Kr.

It has also been suggested on the basis of a caloric curve that MF of Au is a first order phase transition [102]. This observation was based on the the fact that the temperature remains constant as energy is increased between 3 and 10 MeV/nucleon. The temperature again starts increasing beyond 10 MeV/nucleon as a gas phase consisting of a mixture of nucleons and few light particles is created. According to SMM there are few nucleons in the hot system. Fig.24 shows a plot of first moments of the fragment yield distribution as a function of E^*_{th} for Au, La and Kr. The figure shows that even for $E^*_{th} \geq 10$ MeV/nucleon very few particles with $A \leq 4$ are produced. Most of the remnant mass is in fragments with $A > 4$. This argues against the coexistence of the constant density liquid and gas phases

in SMM. The cooling of the hot fragments produces a large number of final state nucleons and light particles as shown in Fig.25. The IMFs survive the cooling process at least for Au and La and identify the MF transition. In case of Kr the excitation energies of IMF from SMM_{hot} are very high and very few are seen in the cold stage. Thus the MF signal could be washed out.

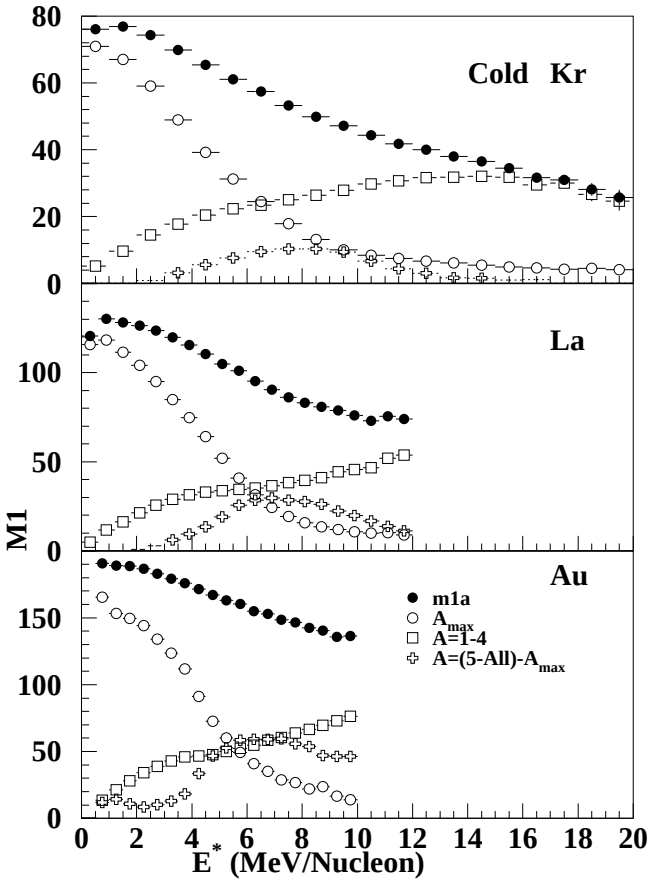

FIG. 25. M1 distribution for SMM_{cold} for Au, La and Kr.

IX. SUMMARY AND CONCLUSIONS

In the present work we presented and analyzed the data from the MF of 1A GeV Au, La and Kr on carbon. The mass, charge and excitation energy of the remnant were determined in each event. The thermal excitation energy was obtained after the expansion energy was determined on the basis of energy balance. The multiplicity distribution from MF of Kr shows a saturation beyond E^*_{th} of 8 MeV/nucleon, indicating that the vaporization process

has started.

A comparison of the data with the variable volume version of SMM, using the same values of parameters of the model for Au, La and Kr show a very good agreement with various distributions e. g. charged particle multiplicity, size of biggest fragment, number of IMFs, etc. The power law behavior seen in data for Au and La with $\tau > 2$ is also observed in SMM when cold fragments are analyzed. The hot fragment analysis from SMM_{hot} for γ_2 gives a value of E_c^* which is in agreement with the value of E_c^* obtained from SMM_{cold}.

The Au and La data give indications of a continuous phase transition. A first order phase transition has been predicted for Kr using SMM. However, the data cannot be used to distinguish between the two because of finite size effects.

The SMM calculation offers the best way to determine the the nature of phase transition. A back bending in temperature vs energy plot is a sign of negative specific heat and hence a first order phase transition. Such a result is found for Kr but not for Au, except for the lightest remnants, the MF contribution of which is negligible.

The temperature obtained from the isotope ratio analysis decreases with an increase in system size at the critical point. The break-up temperature obtained from SMM also follows the same trend, but higher by ~ 1 MeV/nucleon. The decrease in temperature with increase in system size is an important result as it is in the opposite direction from what is observed in either in 3D percolation or Ising model studies for finite size neutral matter. This shows that if finite size were the only effect in MF then the correlation between temperature and system size would have been the same in data as in percolation and Ising model studies. Thus, the long range Coulomb force is shown to be the dominant factor in MF. This conclusion is also supported by Hartree-Fock calculations.

In conclusion, this is the first work in which the nature of the phase transition in MF has been explored using three systems of different size. The experimental results in conjunction with SMM provide the order of the phase transition in Au, La and Kr. The values of critical exponents τ, β and γ, which are close to the values for liquid-gas system, along with nearly zero latent heat suggest a continuous phase transition in Au and La. The back bending in

the caloric curve for Kr suggests the presence of latent heat, which is consistent with a first order phase transition. We emphasize again here the important role played by the Coulomb energy. The Coulomb expansion energy reduces or eliminates the latent heat and changes the nature of the phase transition.

This work was supported by the U. S. Department of Energy.

REFERENCES

[1] D. H. E. Gross ,Rep. Prog. Phys. **53**, 605 (1990).

[2] L. G. Moretto and G. J. Wozniak **43**, 379 (1993).

[3] J. Bondorf *et al.*, Phys. Rep. **257**, 133 (1995).

[4] D. H. E. Gross , Phys. Rep. **279**, 119 (1997).

[5] J. Richert and P. Wagner, Phys. Rep. **350**, 1 (2001).

[6] A. Bonasera *et al*, La Rivista del Nuovo Cimento, della Societ *à* Italiana di Fisica(2000).

[7] S. Das Gupta, A. Z. Mekjian, and M. B. Tsang , nucl-th/0009033.

[8] J. E. Finn *et al*, Phys. Rev. Lett. **49**, 1321 (1982).

[9] R. W. Minich *et al*, Phys. Lett. B**118**, 458 (1982).

[10] M. E. Fisher, Physics **3**, 255 (1967).

[11] P. J. Siemens, Nature **305**, 410 (1983).

[12] T. J. Schalgel and V. R. Pandharipande, Phys. Rev. C **36**, 162 (1987).

[13] H. Muller, and B. D. Serot, Phys. Rev. C **52**, 2072 (1995).

[14] K. C. Chase and Z. Mekjian, Phys. Rev. Lett. **75**, 4732 (1995).

[15] A. M. Poskanzer *et al*, Phys. Rev. C **3**, 882 (1971).

[16] G. D. Westfall *et al*, Phys. Rev. C **17**, 1368 (1978).

[17] A. S. Hirsch *et al*, Phys. Rev. C **29**, 508 (1984).

[18] M. Mahi *et al*, Phys. Rev. Lett. **60**, 1936 (1988).

[19] N. T. Porile *et al*, Phys. Rev. C **39**, 1914 (1989).

[20] C. J. Waddintgton and P. S. Freier , Phys. Rev. C **31**, 888 (1985).

[21] X. Campi, J. Phys. A **19**, L917 (1986).

[22] X. Campi, Phys. Lett. B **208**, 351 (1988).

[23] X. Campi, Proceedings of the International School of Physics 'Enrico Fermi' Nuclear Collisions from the Mean-Field into the Fragmentation regime,**CXII** 331 (1991).

[24] W. Bauer *et al.*, Phys. Lett. B**150**, 53 (1985).

[25] W. Bauer *et al.*, Nucl. Phys. A**452**, 699 (1986).

[26] D. Stauffer, Phys. Rep. **54**, 1 (1979).

[27] D. Stauffer and A. Aharony, Introduction to Percolation Theory (Taylor and Francis , London, 1992).

[28] J. Hubele *et al*, Z. Phys. A **340**, 263 (1991).

[29] P. Kreutz *et al*, Nucl. Phys. A **556**, 672 (1993).

[30] A. Schuttauf *et al*, Nucl. Phys. A **607**, 457 (1996).

[31] U. Jahnke *et al.*, Phys. Rev. Lett. **83**, 4959 (1999).

[32] W.-C. Hsi *et al.*, Phys. Rev. Lett. **79**, 817 (1997).

[33] L. Beaulieu *et al.*, Phys. Lett. **163B**, 159 (1999).

[34] T. Lefort *et al.*, Phys. Rev. C**64**, 064603 (2001).

[35] M. Kleine Berkenbusch *et al.*, Phys. Rev. Lett. **88**, 022701 (2002).

[36] M. L. Gilkes *et al.*, Phys. Rev. Lett. **73**, 1590 (1994).

[37] J. A. Hauger *et al.*, Phys. Rev. Lett. **77**, 235 (1996).

[38] J. B. Elliott *et al.*, Phys. Lett. B**381**, 35 (1996).

[39] J. A. Hauger *et al.*, Phys. Rev. C**57**, 764 (1998).

[40] J. B. Elliott *et al.*, Phys. Lett. B**418**, 34 (1998).

[41] J. Lauret *et al.*, Phys. Rev. C**57**, R1051 (1998).

[42] B. K. Srivastava *et al.*, Phys. Rev. C**60**, 064606 (1999).

[43] J. B. Elliott *et al.*, Phys. Rev. C**62**, 064603 (2000).

[44] J. B. Elliott *et al.*, Phys. Rev. Lett. **85**, 1194 (2000).

[45] J. A. Hauger *et al.*, Phys. Rev.C**62**, 024616 (2000).

[46] B. K. Srivastava *et al.* Phys. Rev. C**64**, 041901(R) (2001).

[47] R. P. Scharenberg *et al.*, Phys. Rev.C **64**, 054602 (2001).

[48] J. Bondorf *et al.*, Nucl. Phys. A **443**, 321 (1985).

[49] J. Bondorf *et al.*, Nucl. Phys. A **444**, 460 (1985).

[50] J. Bondorf *et al.*, Nucl. Phys. A **475**, 663 (1987).

[51] W. A. Friedman, Phys. Rev. C**42**, 467 (1990).

[52] D. Durand, Nucl. Phys. A **541**, 266 (1992).

[53] K. C. Chase and A. Z. Mekjian, Phys. Rev. C **49**, 2164 (1994).

[54] K. C. Chase, A. Z. Mekjian, and P. Bhattacharya, Phys. Rev. C **55**, 1410 (1997).

[55] S. J. Lee and A. Z. Mekjian, Phys. Rev. C **56**, 2621 (1997).

[56] S. Das Gupta and A. Z. Mekjian, Phys. Rev. C **57**, 1361 (1998).

[57] W. Bauer, Phys. Rev. C**38**, 1297 (1988).

[58] J. Pan and S. Das Gupta, Phys. Rev. C **51**, 1384 (1995).

[59] X. Campi and H. Krivine, Nucl. Phys. A **620**, 46 (1997).

[60] S. Das Gupta *et al.*, Nucl. Phys. A **621**, 897 (1997).

[61] J. Pan and S. Dasgupta, Phys. Rev. Lett. **80**, 1182 (1998).

[62] J. M. Carmona *et al.*, Nucl. Phys. A **643**, 115 (1998).

[63] F. Gulminelli and Ph. Chomaz, Phys. Rev. Lett. **82**, 1402 (1999).

[64] A. L. Goodman *et al.*, Phys. Rev. C **30**, 851 (1984).

[65] R. P. Scharenberg, Proceedings of the International Workshop XXVII on Gross Properties of Nuclei and Nuclear Excitations, Hirschegg, Austria, p 237 , GSI 1999.

[66] B. K. Srivastava, Proceedings of the International Workshop XXVII on Gross Properties of Nuclei and Nuclear Excitations, Hirschegg, Austria, p 247 , GSI 1999.

[67] G. Rai *et al.*, IEEE Trans. Nucl. Sci. **37**, 56 (1990).

[68] H. Wieman *et al.*, Nucl. Phys. A **525**, 617c (1991).

[69] G. Bauer *et al.*, Nucl.Instr. Metds. Phys. Res. A **386**, 249 (1997).

[70] Y. Yariv and Z. Fraenkel, Phys. Rev. C**20**, 2227 (1979).

[71] Y. Yariv and Z. Fraenkel, Phys. Rev. C**24**, 488 (1981).

[72] D. Cussol *et al.*, Nucl. Phys. A **561**, 298 (1993).

[73] L. Beaulieu *et al.*, Phys. Rev.C**54**, R973 (1996).

[74] I. N. Mishustin, Nucl. Phys. A **630**, 111c (1998).

[75] D. G. Ravenhall *et al.*, Nucl. Phys. A **407**, 572 (1983).

[76] J. B. Elliott *et al.*, Phys. Rev. C**49**, 3185 (1994).

[77] J. B. Elliott *et al.*, Phys. Rev. C**55**, 1319 (1997).

[78] Bao-An Li *et al.*, Phys. Lett. B**303**, 225 (1993).

[79] H. W. Barz *et al.*, Nucl. Phys. A **561**, 466 (1993).

[80] M. Belkacem *et al.*, Phys. Rev. C**54**, 2435 (1996).

[81] P. F. Mastinu *et al.*, Phys. Rev. C**57**, 831, (1998).

[82] M. D'Agostino *et al.*, Nucl. Phys. A **650**, 329 (1999).

[83] X. Campi and H. Krivine, Nucl. Phys. A **545**, 161c (1992).

[84] X. Campi and H. Krivine, Z. Phys. A**344**, 81 (1992).

[85] H. R. Jaqaman and D. H. E. Gross, Nucl. Phys. A **524**, 321 (1991).

[86] M. Belkacem *et al.* Phys. Rev. C**52**, 271 (1995).

[87] H. E. Stanley, Introduction to phase transition and critical phenomena, (Clarendon, Oxford, 1971).

[88] M. N. Barber, Phase tensitions and critical phenomena, Vol.8 , Eds. C. Domb and J. L. Lebowitz (Academic press Inc., London,1983).

[89] G. Grimmett, Percolation, (Springer, New York, 1989).

[90] J. M. Yeomans, Statistical mechanics of phase transitions,(Clarendo, Oxford, 1993).

[91] X. Campi, Nucl. Phys. A**495**, 259c (1989).

[92] Ph. Chomaz and F. Gulminelli, Nucl. Phys. A **647**, 153 (1999).

[93] M. D'Agostino *et al*, Phys. Lett. B **473**, 219 (2000).

[94] A. Huller , Z. Phys. B **93**, 401 (1994).

[95] J. B. Natowitz *et al.* , nucl-ex/0106016.

[96] S. Albergo *et al.*, Nuovo Cimento A**89**, 1 (1985).

[97] D. W. Heerman and D. Stauffer , Z. Phys.**B44**, 339 (1981).

[98] H. R. Jaqaman *et al.*, Phys. Rev. C**29**, 2067 (1984).

[99] P. Bonche *et al.*, Nucl. Phys. **A436**, 265 (1985).

[100] S. Levit and P. Bonche , Nucl. Phys. **A437**, 426 (1985).

[101] J. M. Lattimer *et al.*, Nucl. Phys. **A432**, 646 (1985).

[102] J. Pochodzalla et al., Phys. Rev. Lett.**75**, 1040 (1995).